Electronic Supplementary Material (ESI) for Inorganic Chemistry Frontiers.

Supporting Information

Poly(3,4-ethylenedioxythiophene) Encapsulating Hydrated Vanadium Oxide Nanobelts Boosts their Conductivity and Zinc-ion Storage Properties

Jingjing Sun[1], Mengyu Rong[1], Zhanming Gao[2], Ziyi Feng[1], Yanyan Liu[1], Tao Hu[1,*], Changgong Meng[1,3], Yifu Zhang[1,*]

[1]*School of Chemistry, Dalian University of Technology, Dalian, 116024, China*

[2]*State Key Laboratory of Fine Chemicals, School of Chemical Engineering, Dalian University of Technology, Dalian, 116024, China*

[3]*College of Environmental and Chemical Engineering, Dalian University, Dalian, 116622, China*

*Corresponding authors.

Tao Hu: inorchem@dlut.edu.cn; Yifu Zhang: yfzhang@dlut.edu.cn

Materials

Ammonium metavanadate (NH_4VO_3, 99%) and glacial acetic acid (HOAc, 99.5%) were purchased from the Siopharm Chemical Reagent Co., Ltd. 3,4-ethylenedioxythiophene (EDOT) monomer was purchased from the Tianjin Damao Chemical Reagent Factory. All materials were used as received without any further treatment.

Fig. S1

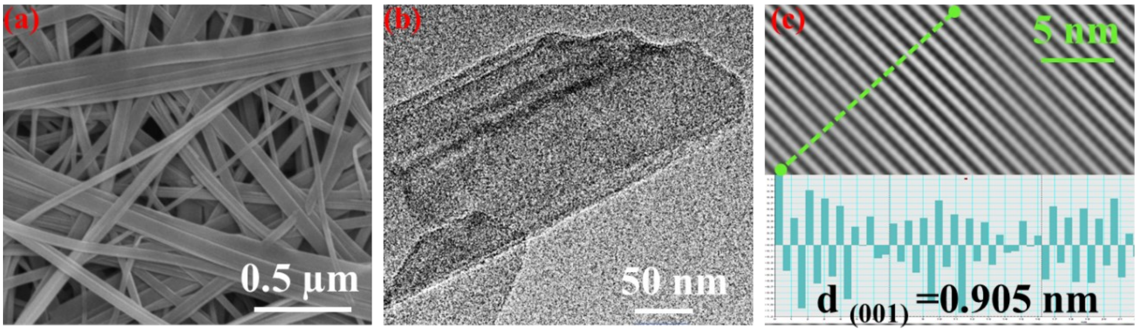

Fig. S1. Morphology of VOH: **a** SEM image; **b** TEM image; **c** HRTEM image and corresponding lattice distance.

Fig. S2

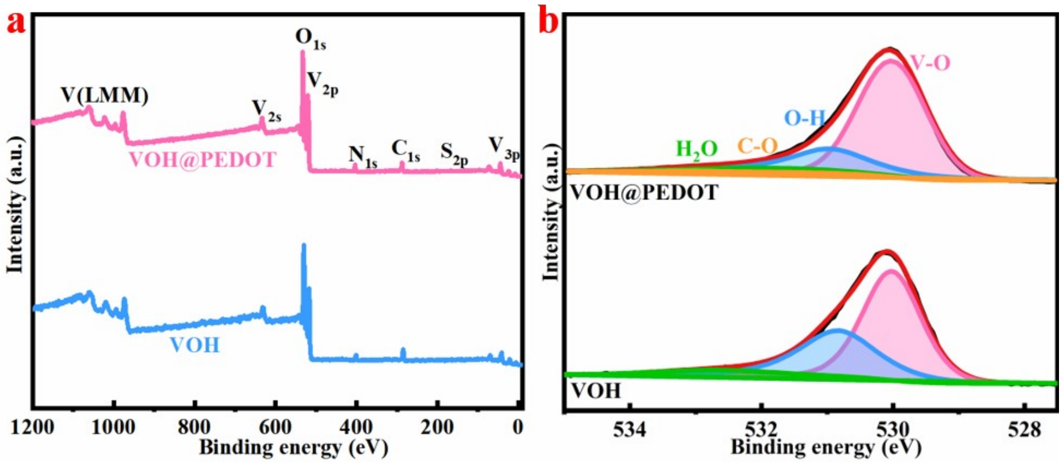

Fig. S2. a XPS survey spectra and **b** high-resolution O 2p XPS spectra of VOH and VOH@PEDOT.

Fig. S3

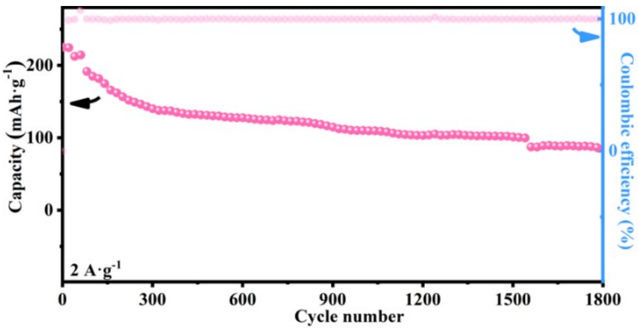

Fig. S3. Cycling performance of Zn//VOH@PEDOT cell at 0.1 A g^{-1}

Fig. S4

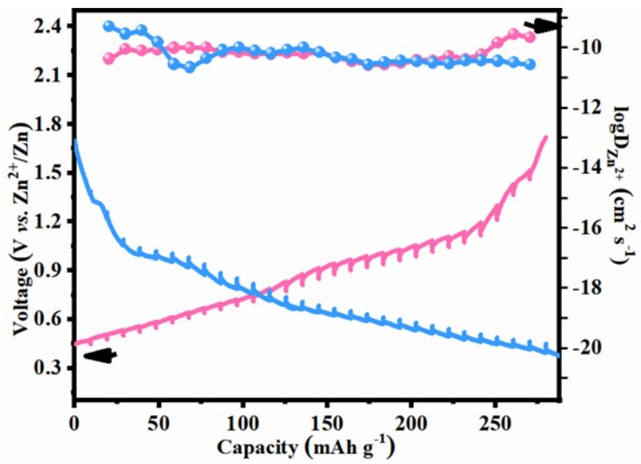

Fig. S4. GITT curves and the diffusion coefficients of the Zn//VOH cell at charge/discharge states.

Fig. S5

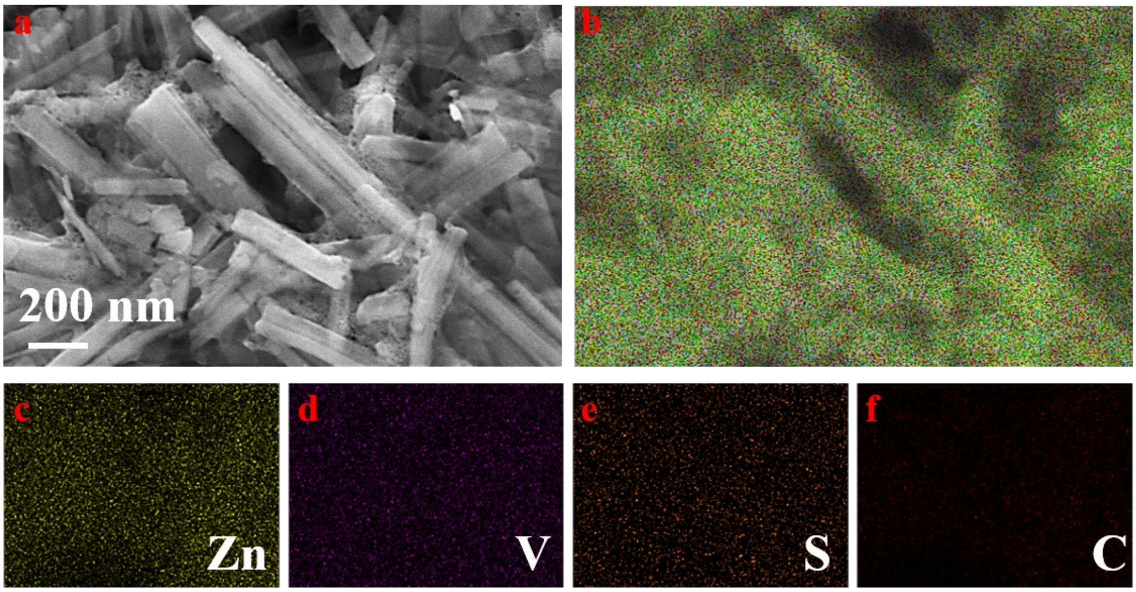

Fig. S5. a SEM image of VOH@PEDOT after long cycles. **b-f** Elemental mapping images of VOH@PEDOT.

Fig. S6

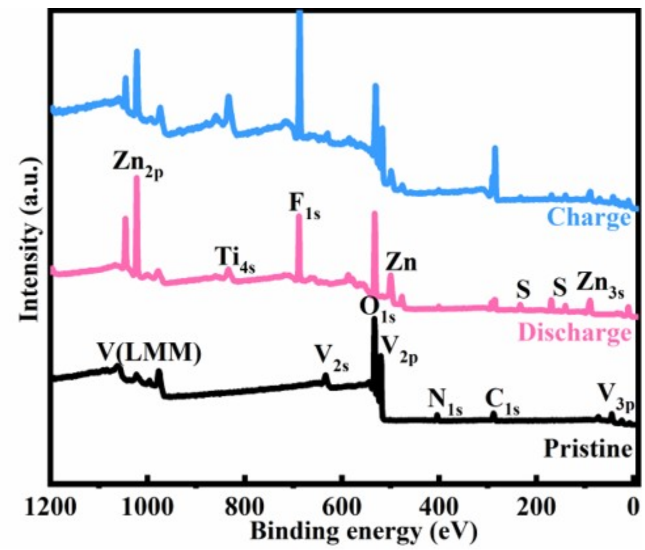

Fig. S6. XPS survey spectra of VOH@PEDOT at different states.

Fig. S7

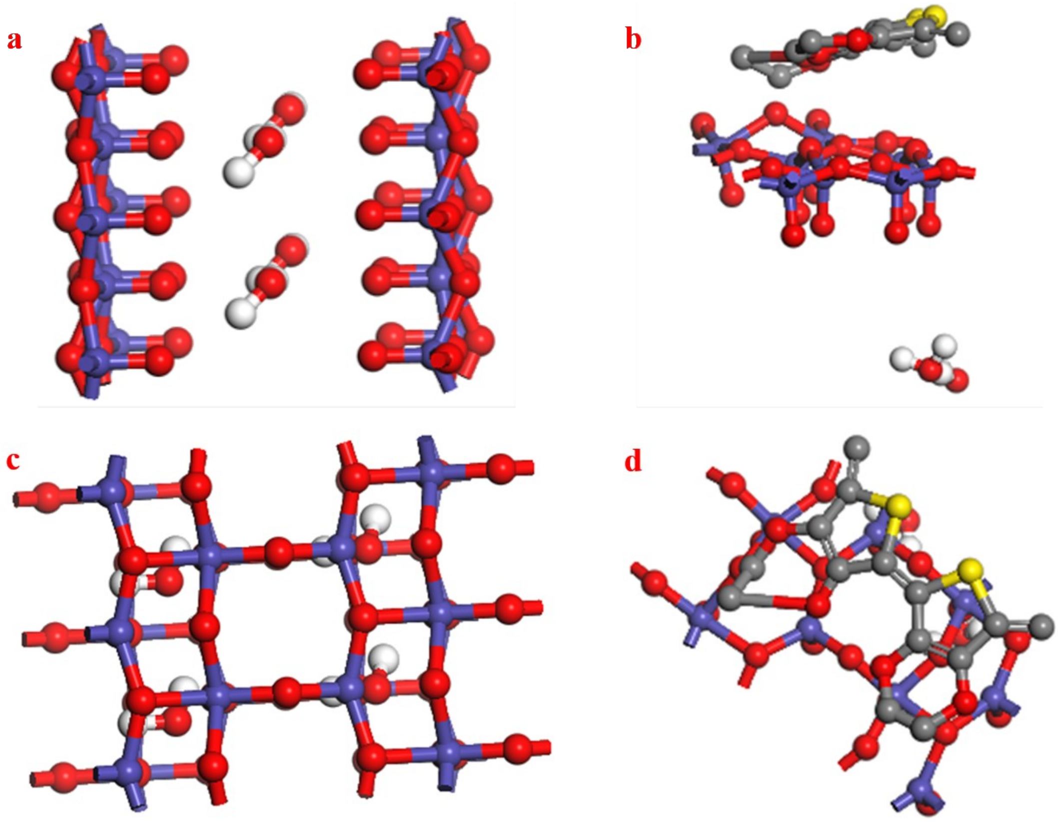

Fig. S7. Structural side and top views of VOH (**a** and **c**) and VOH@PEDOT (**b** and **d**).

Fig. S8

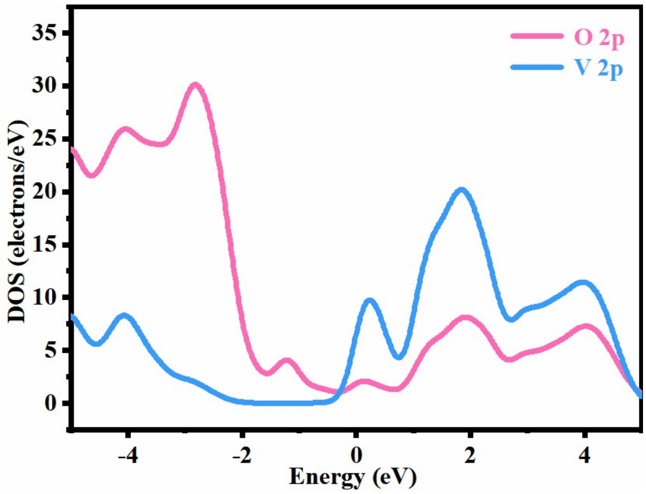

Fig. S8. DOS of O 2p and C 2p orbitals for VOH@PEDOT.

Table S1

Table S1. Detailed information on the peak position and intensity of high-resolution V 2p spectra of VOH and VOH@PEDOT in various states.

Material	Information	V^{5+} ($2p_{1/2}$)	V^{4+} ($2p_{1/2}$)	V^{3+} ($2p_{1/2}$)	V^{5+} ($2p_{3/2}$)	V^{4+} ($2p_{3/2}$)	V^{3+} ($2p_{3/2}$)
VOH	Position (eV)	525.2	524.5	523.8	517.8	517.4	516.1
	Area	5856.55	1213.77	7110.5	11538.3	11867.4	9881.2
	Proportion (%)	12	2.6	15	24.3	25	21
VOH@PEDOT (pristine)	Position (eV)	525.2	524.5	523.8	517.8	517.3	516.1
	Area	8740	5374.2	17751	23416.8	29538.6	19693.4
	Proportion (%)	8.4	5	1.7	22.4	28.3	18.8
VOH@PEDOT (discharged)	Position (eV)	525.2	524.5	523.8	517.8	516.9	516.1
	Area	474.3	932.6	3700	2038.4	1349.2	1555
	Proportion (%)	4.7	9.3	37	20.3	13.4	15.5
VOH@PEDOT (charged)	Position (eV)	525.2	524.5	523.8	517.8	517.3	516.3
	Area	5018.2	827	6908.3	11468.5	13837.4	2440
	Proportion (%)	12	2	17	28	34.2	6

Table S2

Table S2. Comparison of the electrochemical performance of other aqueous zinc-ion batteries with similar cathode materials with the Zn//VOH@PEDOT cell

Cathode materials	Specific capacity	Cycling	Energy density	Power density	Ref.
VO_2(B) nanofibers	357 mAh g^{-1} at 0.1 A g^{-1}	~100% after 50 cycles at 0.1 A g^{-1}	297 Wh kg^{-1}	180 W kg^{-1}	1
VO_2/rGO composite	276 mAh g^{-1} at 0.1 A g^{-1}	99% after 1000 cycles at 4 A g^{-1}	65 Wh kg^{-1}	7800 W kg^{-1}	2
$H_2V_3O_8$ nanowire/Graphene	394 mAh g^{-1} at 0.1 A g^{-1}	-	89 Wh kg^{-1}	2215 W kg^{-1}	3
$V_{10}O_{24}\cdot 12H_2O$	164.5 mAh g^{-1} at 0.2 A g^{-1} after 2 cycles	81.6% after 1000 cycles at 5 A g^{-1}	163.4 Wh kg^{-1}	217.9 W kg^{-1}	4
$V_2O_5\cdot nH_2O$/graphene	381 mAh g^{-1} at 0.3 A g^{-1}	71% after 900 cycles at 6 A g^{-1}	90 Wh kg^{-1}	6400 W kg^{-1}	5
CaVOH/rGO	409 mAh g^{-1} at 0.05 A g^{-1}	90% over 2000 cycles at 4 A g^{-1}	381 Wh kg^{-1}	48 W kg^{-1}	6
PANI-$V_2O_5\cdot nH_2O$	363 and 143 mAh g^{-1} at 0.1 and 4 A g^{-1}	196 mAh g^{-1} left over 100 cycles at 5 A g^{-1}	275 Wh kg^{-1}	78 W kg^{-1}	7
PANI-$V_2O_5\cdot nH_2O$	350 mAh g^{-1} at 0.1 A g^{-1}	-	-	-	8
PANI-$V_2O_5\cdot nH_2O$	380 mAh g^{-1} at 0.1 A g^{-1}	259 mAh g^{-1} left over 800 cycles at 1 A g^{-1}	216 Wh kg^{-1}	252 W kg^{-1}	9
PANI/V_2O_5	353.6 mAh g^{-1} at 0.1A g^{-1}	280 mAh g^{-1} left over 100 cycles at 0.2 A g^{-1}	258 Wh kg^{-1}	2784 W kg^{-1}	10
PANI-V_2O_5	360 mAh g^{-1} at 0.5 A g^{-1}	208 mAh g^{-1} left over 2000 cycles at 5 A g^{-1}	187 Wh kg^{-1}	7200 W kg^{-1}	11
Rose-like PANI-intercalated V_2O_5	420 mAh g^{-1} at 0.5 A g^{-1}	87.5% left over 600 cycles at 5 A g^{-1}	-	-	
PANI-intercalated V_2O_5	490 mAh g^{-1} at 0.1 A g^{-1}	201 mAh g^{-1} left over 1000 cycles at 2 C	430 Wh kg^{-1}	-	11
V_2O_5/PEDOT	380, 274 and 102 mAh g^{-1} at 0.3, 5 and 20 A g^{-1}	93% capacity left over 200 cycles at 5 A g^{-1}	-	-	12
PANI-VOH@PANI			576.8 Wh kg^{-1}	84.1 W kg^{-1}	13
PEDOT intercalated VOH	370.5 and 175 mAh g^{-1} at 0.5 and 50 A g^{-1}	310.1 mAh g^{-1} left over 1000 cycles at 5 A g^{-1}	-	-	14
PEDOT intercalated Vö- V_2O_5	449 mAh g^{-1} at 0.2 A g^{-1}	94.3% capacity left over 6000	302 Wh kg^{-1}	60 W kg^{-1}	15

		cycles at 10 A g^{-1}			
PEDOT intercalated V_2O_5	388, 367 and 351 mAh g^{-1} at 5, 8 and 10 A g^{-1}	269 mAh g^{-1} left over 4500 cycles at 10 A g^{-1}	247.57 Wh kg^{-1}	590.8 W kg^{-1}	16
PEDOT-$NH_4V_3O_8$	356.8 and 163.6 mAh g^{-1} at 0.05 and 10 A g^{-1}	94.1% capacity left over 5000 cycles at 10 A g^{-1}	353.1 Wh kg^{-1}	50 W kg^{-1}	17
V_2O_5@PEDOT on carbon cloth	360 and 232 mAh g^{-1} at 0.1 and 20 A g^{-1}	97% capacity left over 600 cycles at 1 A g^{-1} 89% capacity left over 1000 cycles at 5 A g^{-1}	243.3 Wh kg^{-1}	90 W kg^{-1}	18
VOH@PEDOT	432 mAh g^{-1} at 0.1 A g^{-1}	323 mAh g^{-1} left over 100 cycles at 0.1 A g^{-1}	255 Wh kg^{-1}	245 W kg^{-1}	This work

Table S3

Table S3. Detailed information on the peak position and intensity of high-resolution C 1s spectra of VOH@PEDOT in various states.

State	Information	C-O	C-S	C=C	C-C
Pristine	Position (eV)	288.24	286.06	284.77	284.1
	Area	1191.3	4467.5	4488.2	1465.3
	Proportion (%)	10.3	38.6	38.75	12.4
Discharged	Position (eV)	288.24	286.4	284.77	284.1
	Area	4045.2	13339.8	12251	6760.2
	Proportion (%)	11.1	36.7	33.7	17.2
Charged	Position (eV)	288.24	286.06	284.77	284.1
	Area	1403.2	13046.4	11765.8	913.6
	Proportion (%)	5.2	49.1	44.1	3.4

References

1. J. Ding, Z. Du, L. Gu, B. Li, L. Wang, S. Wang, Y. Gong and S. Yang, Ultrafast Zn^{2+} Intercalation and Deintercalation in Vanadium Dioxide, *Adv. Mater.*, 2018, **30**, 1800762.

2. X. Dai, F. Wan, L. Zhang, H. Cao and Z. Niu, Freestanding graphene/VO_2 composite films for highly stable aqueous Zn-ion batteries with superior rate performance, *Energy Storage Mater.*, 2019, **17**, 143-150.

3. Q. Pang, C. Sun, Y. Yu, K. Zhao, Z. Zhang, P. M. Voyles, G. Chen, Y. Wei and X. Wang, $H_2V_3O_8$ Nanowire/Graphene Electrodes for Aqueous Rechargeable Zinc Ion Batteries with High Rate Capability and Large Capacity, *Adv. Energy Mater.*, 2018, **8**, 1800144.

4. T. Wei, Q. Li, G. Yang and C. Wang, High-rate and durable aqueous zinc ion battery using dendritic $V_{10}O_{24}\cdot 12H_2O$ cathode material with large interlamellar spacing, *Electrochim. Acta*, 2018, **287**, 60-67.

5. M. Yan, P. He, Y. Chen, S. Wang, Q. Wei, K. Zhao, X. Xu, Q. An, Y. Shuang, Y. Shao, K. T. Mueller, L. Mai, J. Liu and J. Yang, Water-Lubricated Intercalation in $V_2O_5\cdot nH_2O$ for High-Capacity and High-Rate Aqueous Rechargeable Zinc Batteries, *Adv. Mater.*, 2018, **30**, 1703725.

6. T. Hu, Z. Feng, Y. Zhang, Y. Liu, J. Sun, J. Zheng, H. Jiang, P. Wang, X. Dong and C. Meng, "Double Guarantee Mechanism" of Ca^{2+}-intercalation and rGO-integration Ensures Hydrated Vanadium Oxide with a High Performance for Aqueous Zinc-ion Batteries, *Inorg. Chem. Front.*, 2021, **8**, 79-89.

7. Y. Zhang, L. Xu, H. Jiang, Y. Liu and C. Meng, Polyaniline-expanded the interlayer spacing of hydrated vanadium pentoxide by the interface-intercalation for aqueous rechargeable Zn-ion batteries, *J. Colloid Interface Sci.*, 2021, **603**, 641-650.

8. R. Li, F. Xing, T. Li, H. Zhang, J. Yan, Q. Zheng and X. Li, Intercalated polyaniline in V_2O_5 as a unique vanadium oxide bronze cathode for highly stable aqueous zinc ion battery, *Energy Storage Mater.*, 2021, **38**, 590-598.

9. M. Wang, J. Zhang, L. Zhang, J. Li, W. Wang, Z. Yang, L. Zhang, Y. Wang, J. Chen, Y. Huang, D. Mitlin and X. Li, Graphene-like Vanadium Oxygen Hydrate (VOH) Nanosheets Intercalated and Exfoliated by Polyaniline (PANI) for Aqueous Zinc-Ion Batteries (ZIBs), *ACS Appl. Mater. Interfaces*, 2020, **12**, 31564-31574.

10. Y. Liu, Z. Pan, D. Tian, T. Hu, H. Jiang, J. Yang, J. Sun, J. Zheng, C. Meng and Y. Zhang, Employing "one for two" strategy to design polyaniline-intercalated hydrated vanadium oxide with expanded interlayer spacing for high-performance aqueous zinc-ion batteries, *Chem. Eng. J.*, 2020, **399**, 125842.

11. S. Chen, K. Li, K. S. Hui and J. Zhang, Regulation of Lamellar Structure of Vanadium Oxide via

Polyaniline Intercalation for High-Performance Aqueous Zinc-Ion Battery, *Adv. Funct. Mater.*, 2020, **30**, 2003890.

12. F. S. Volkov, E. G. Tolstopjatova, S. N. Eliseeva, M. A. Kamenskii, A. I. Vypritskaia, A. I. Volkov and V. V. Kondratiev, Vanadium(V) oxide coated by poly(3,4-ethylenedioxythiophene) as cathode for aqueous zinc-ion batteries with improved electrochemical performance, *Mater. Lett.*, 2022, **308**, 131210.

13. J. Sun, Y. Zhao, Y. Liu, H. Jiang, C. Huang, M. Cui, T. Hu, C. Meng and Y. Zhang, "Three-in-One" Strategy that Ensures $V_2O_5{\cdot}nH_2O$ with Superior Zn^{2+} Storage by Simultaneous Protonated Polyaniline Intercalation and Encapsulation, *Small Struct.*, 2022, **3**, 2100212.

14. S. Li, X. Wei, C. Wu, B. Zhang, S. Wu and Z. Lin, Constructing Three-Dimensional Structured V_2O_5/Conductive Polymer Composite with Fast Ion/Electron Transfer Kinetics for Aqueous Zinc-Ion Battery, *ACS Appl. Energ. Mater.*, 2021, **4**, 4208-4216.

15. Y. Du, X. Wang and J. Sun, Tunable oxygen vacancy concentration in vanadium oxide as mass-produced cathode for aqueous zinc-ion batteries, *Nano Res.*, 2021, **14**, 754-761.

16. Z. Yao, Q. Wu, K. Chen, J. Liu and C. Li, Shallow-layer pillaring of a conductive polymer in monolithic grains to drive superior zinc storage via a cascading effect, *Energ. Environ. Sci.*, 2020, **13**, 3149-3163.

17. D. Bin, W. Huo, Y. Yuan, J. Huang, Y. Liu, Y. Zhang, F. Dong, Y. Wang and Y. Xia, Organic-Inorganic-Induced Polymer Intercalation into Layered Composites for Aqueous Zinc-Ion Battery, *Chem*, 2020, **6**, 968-984.

18. D. Xu, H. Wang, F. Li, Z. Guan, R. Wang, B. He, Y. Gong and X. Hu, Conformal Conducting Polymer Shells on V_2O_5 Nanosheet Arrays as a High-Rate and Stable Zinc-Ion Battery Cathode, *Adv. Mater. Interfaces*, 2019, **6**, 1801506.